Three-dimensional magnetic field topology in a region of solar coronal heating

S. K. Solanki[1], A. Lagg[1], J. Woch[1], N. Krupp[1] & M. Collados[2]

[1]*Max-Planck-Institut für Aeronomie, 37191 Katlenburg-Lindau, Germany*
[2]*Instituto de Astrofísica de Canarias, La Laguna, Tenerife, Spain*

Flares and X-ray jets on the Sun arise in active regions where magnetic flux emerges from the solar interior amd interacts with the ambient magnetic field[1,2]. The interactions are believed to occur in electric current sheets separating regions of opposite magnetic polarity. The current sheets located in the corona or upper chromosphere have long been thought to act as an important source of coronal heating[3–6], requiring their location in the corona or upper chromosphere. The dynamics and energetics of these sheets are governed by a complex magnetic field structure that, until now, has been difficult to measure. Here we report the determination of the full magnetic vector in an interaction region near the base of the solar corona. The observations reveal two magnetic features that characterize young active regions on the Sun: a set of rising magnetic loops and a tangential discontinuity of the magnetic field direction, the latter being the observational signature of an electric current sheet. This provides strong support for coronal heating models based on the dissipation of magnetic energy at current sheets.

The analysed observations were recorded on 13 May 2001 with the Tenerife Infrared Polarimeter (TIP)[7] at the German Vacuum Tower Telescope (VTT) at the Spanish observatory of Izaña, Tenerife. We used observations in the He I 1083.0 nm multiplet[8–11] to create maps of an emerging flux region in all four Stokes parameters *I*, *Q*, *U* and *V*, completely describing the polarized states of light. From the measured Stokes vector we derived the line-of-sight velocities, the strength of the magnetic field, its inclination to the solar surface normal and its direction in the horizontal plane (that is, the azimuth angle) in the photosphere and upper chromosphere. These parameters are plotted in Fig. 1. Within the scanned region the magnetic field changes its polarity from outward (away from the Sun, inclination angle close to 0°) in the East (left) to the opposite polarity in the West. On a scale larger than 10×10^6 m the shape and position of the boundary between the two polarities is similar in both layers. On smaller scales there are considerable deviations, with a strongly undulating boundary in the photosphere, including localized patches of opposite-polarity fields

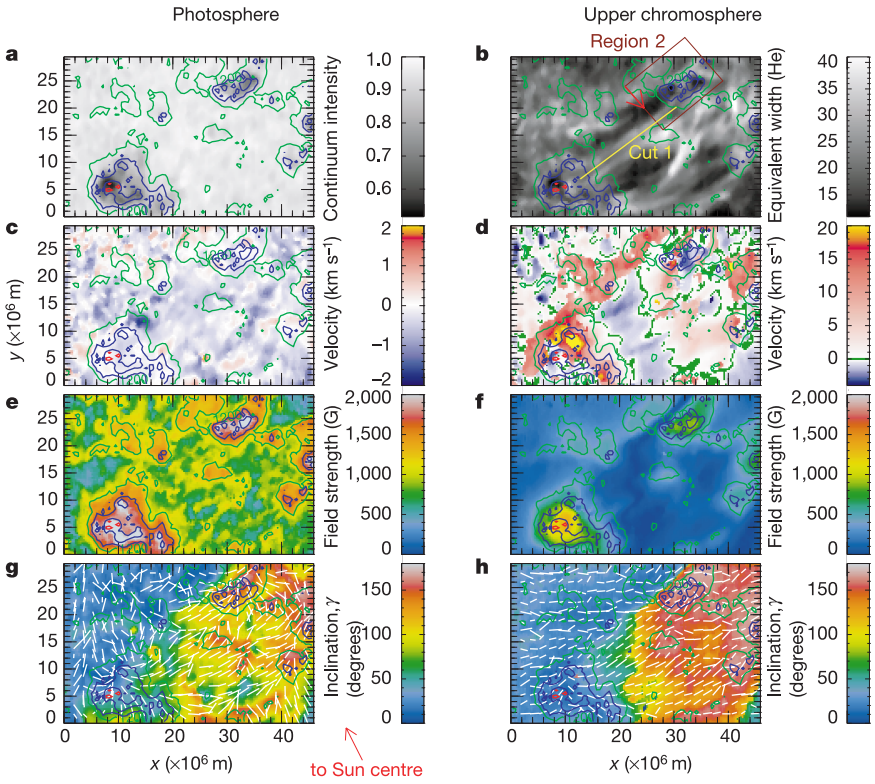

Figure 1 Atmospheric parameters of an emerging flux region (NOAA active region 9451, 33°W, 22°S). Displayed are from top to bottom continuum intensity (**a**) and the equivalent width of He I 1083.0 nm (**b**), the line-of-sight velocity, magnetic field strength and zenith angle (colour scale) with overplotted azimuthal direction (white lines). The photospheric maps (**a**, **c**, **e**, **g**) are derived from the measured Stokes profile of the Si I 1082.7 nm line (effective Landé factor $g_{\text{eff}} = 1.5$), the upper chromospheric maps (**b**, **d**, **f**, **h**) from the He I triplet at 1082.909 nm ($g_{\text{eff}} = 2.0$), 1083.025 nm ($g_{\text{eff}} = 1.75$) and 1083.034 nm ($g_{\text{eff}} = 0.875$). Positive values of the velocity denote downflows. The contour lines in each panel indicate photospheric magnetic field strength for reference (drawn at 1,200, 1,600, 2,000, 2,400 G). The pixel area is $0.39 \times 0.4''$ and the complete scan, recorded in 146 steps within 12 minutes, provides a field-of-view of $(46 \times 10^6) \times (30 \times 10^6)$ m^2 on the Sun. Owing mainly to turbulence in the Earth's atmosphere the true spatial resolution is approximately 1.5″. The Si I 1082.7 nm line, which is formed under local thermal equilibrium (LTE) conditions, was analysed by applying a response-function based inversion to the Stokes profiles[17,18]. The model atmosphere consists of two components: a magnetic component for which temperature, the magnetic vector and line-of-sight velocity are deduced, and a field-free component corresponding to a quiet Sun model atmosphere[19]. The He I triplet, which has a complex non-LTE line formation[20] but is nearly optically thin[21], was analysed by applying the Unno–Rachkowski solution to describe the individual Zeeman components of each member of the triplet to the data[22] combined with a simple implementation of the Hanle effect based on recent developments[23]. Further details of the analysis are given elsewhere[24].

within the large-scale unipolar regions (visible in Fig. 1g). The magnetic structure is far more ordered in the upper chromosphere. This supports the view that whereas the Si I line basically samples a slab in the atmosphere (the photosphere) the He I triplet, being optically thin, gets contributions from all heights at which sufficient quantities of both neutral helium and ionizing radiation are present. Thus, at different locations within the emerging flux region the He I line is formed at different heights, following the corrugated coronal boundary.

The smooth change of the inclination angle from the upper right to the lower left (of Fig. 1h) deduced from the He triplet (that is, between the two newborn pores or continuum dark structures), suggests that the He I emission originates from loops connecting the two opposite photospheric polarities. This is supported by the fact that the field appears to be following the elongated filaments connecting the two pores seen in Fig. 1b. While a loop is still emerging it carries gas that has not yet been heated to coronal temperatures. Such gas is then visible in radiation absorbed by chromospheric spectral lines such as hydrogen Hα and He I 1083.0 nm.

This interpretation is supported by Fig. 2, in which the components of the magnetic vector and the line-of-sight velocity obtained from He I along the yellow line marked 'Cut 1' in Fig. 1b are plotted. The remarkably smooth variation of the magnetic parameters along this cut is quite evident, with the strength of the field decreasing steadily as it becomes increasingly horizontal. By contrast, the velocity increases from the middle towards both ends. This behaviour is very much like what one would expect when tracing the magnetic vector and the line-of-sight velocity along an emerging loop and projecting these quantities onto a plane. The cut shown in Fig. 2 suggests that the complete freshly emerged loops exhibit He I absorption (and not just their footpoints). These loops have not yet been in the solar atmosphere sufficiently long to let the relatively cool gas at chromospheric temperatures drain out, nor for it to have been heated to higher temperatures. Because the loops are still rising and draining (see Fig. 2c, showing a slow upflow in the centre and rapid, nearly sonic downflows near the edges), the structure is dynamic, so that He I absorption can occur at heights considerably larger than the scale height of chromospheric gas in a static situation.

Using simple criteria it is now possible to reconstruct the full three-dimensional structure of a magnetic loop in the solar atmosphere. The employed approach builds on the regular variation of the magnetic vector and the velocity field across the neutral line of the young active region (as exemplified by Fig. 2). The reconstruction starts by choosing a random pixel and identifying the two neighbouring pixels to which the magnetic azimuth points. If the field measured in these neighbouring pixels matches the field in the initial pixel in direction and strength, then they may belong to the same field line if the additional constraint is satisfied that the field

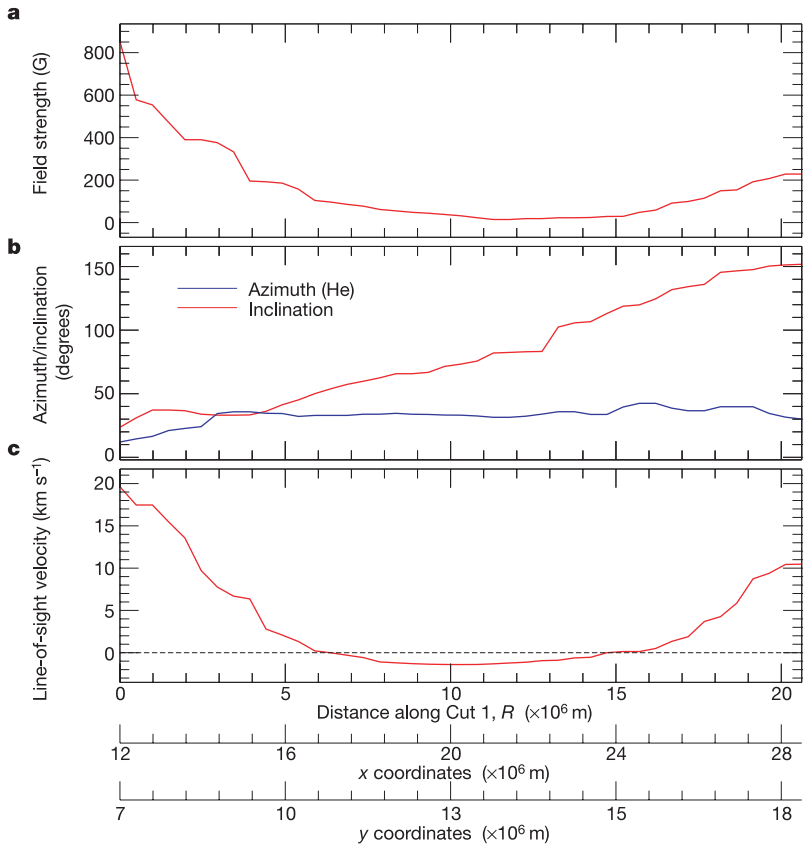

Figure 2 Magnetic and velocity field parameters obtained from the He triplet along 'Cut 1' in Fig. 1. For completeness, the horizontal axis lists the distance along the cut, *R* (top row of numbers), as well as the *x* and *y* coordinates taken from Fig. 1. The magnetic field strength decreases from a maximum value of 840 G at the edge to 20 G at the centre (**a**). The field is almost perpendicular to the solar surface near the edge of the cut (20° and 150° inclination) and is horizontal in the centre (inclination angle 90°, red curve in **b**). In this specific cut the azimuth stays almost constant between 30° and 40° within the achieved accuracy over almost the whole length (**b**). This azimuth implies that the field follows the geometric angle of 'Cut 1'. The plotted magnetic profile is strongly suggestive of a loop. The velocity profile (**c**) shows the typical signature of freshly emerging magnetic flux—an upflow region in the centre (around the loop top) with velocities of 2 km s^{-1} and a drainage of material with downflow velocities of up to 19.6 km s^{-1} on the sides (loop footpoints). The horizontal dotted line represents gas at rest.

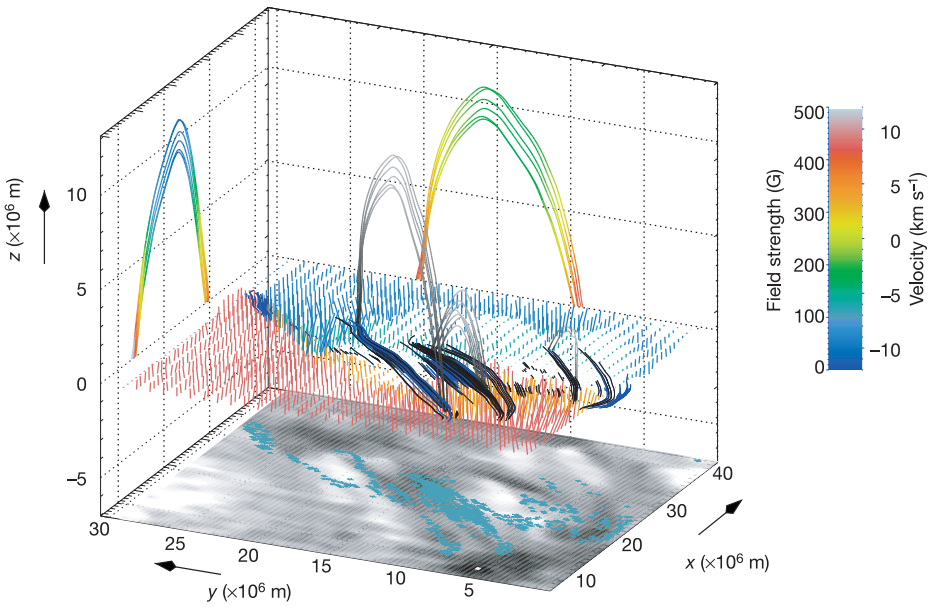

Figure 3 Reconstructed magnetic loops in the emerging flux region. The He I equivalent width map at the bottom is overlaid by a magnetic polarity and connectivity map over which examples of reconstructed loops are plotted. The derived azimuth and inclination angles of the magnetic field in each of the map's pixels are used to trace magnetic field lines. Heavy black lines are projections onto a fixed height of loops fulfilling all the criteria outlined in the text. Gratifyingly, these loops trace the He I equivalent width pattern (shown at the bottom of the plot). Some representative loop field lines are also plotted and for one of the plotted loops they are projected onto the *x*–*z* and *y*–*z* planes. The colour-coding of the loop projections represents the line-of-sight (basically vertical) velocity (*y*–*z* plane) and the magnetic field strength (*x*–*z* plane). The loops are rooted in areas with downflowing material, while in the apex upflowing material is observed. This observation, combined with the frozen-in horizontal magnetic field, implies that the whole loop is rising. The magnetic field strength decreases with height in both legs from about 390 and 500 G at the two chromospheric footpoints to below 50 G at the apex. Magnetic field vectors at the footpoints of the field lines are shown to visualize the overall magnetic field geometry and strength. Field lines out of (or into) the plane parallel to the solar surface are coded in red and orange (or blue and green), with orange and green marking field lines that close within the tracing box, that is, for which both footpoints lie within the observed area and He I emission is seen from the whole length of the loop.

strength decreases with height. The height sampled in the neighbouring pixel relative to that in the original pixel is determined by the magnetic inclination and the size of the pixel. If the field is stronger or points in a distinctly different direction then we expect that the radiation in the two pixels is coming from different loops. Thus, starting from a given pixel, we follow a field line in both directions until one of the above criteria is no longer satisfied. If the end-points of such a field line lie at roughly the same height, have opposite polarities and if neighbouring pixels of one end-point map to neighbouring pixels of the other end-point, then we identify the traced bundle of field lines with a loop. The loops recovered in this manner are three-dimensional structures, because we have information on the full magnetic vector. Examples of reconstructed loops are plotted in Fig. 3. The loops show an asymmetry, such as in the field strength between the two footpoints. The loops fan out as the field strength drops with height (nearly exponentially, with a scale height for the largest loops of 4–5 × 10^6 m). This is in contrast to the very thin, fibril-like loops observed by the Transition Region and Coronal Explorer (TRACE)[12], suggesting that the emission recorded by TRACE selectively highlights a few field lines. Using the deduced loop geometry we determine that the downflows along the loop legs correspond to freely falling material[13].

The maps made in the He I lines reveal locations of strong gradients in the magnetic vector. The strongest gradient lies in the box marked 'Region 2' in Fig. 1. A blow-up of the field strength in this box is displayed in Fig. 4. Clearly, the field strength drops abruptly along the neutral line, forming a deep valley whose width corresponds closely to the estimated spatial resolution of 1.5″. Obviously, this feature has not been fully resolved. The strength of the computed electric current is represented by the colours. Figure 4 strongly suggests that we are dealing here with a current

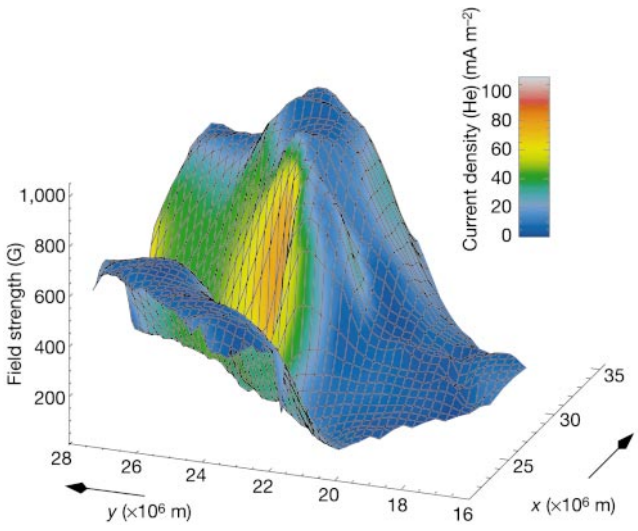

Figure 4 Representation of the electric current sheet (See 'Region 2' in Fig. 1 for the location within the full scanned region). The elevation of the meshed surface is proportional to the magnetic field strength in the upper chromosphere. A narrow valley of low magnetic field values separates two areas of opposite magnetic polarity, so that an electric current flows along this boundary parallel to the solar surface. The colour-coding in the figure indicates the current density of this current sheet calculated using Ampère's law. The maximum value of approximately 90 mA m^{-2} in the region of the largest magnetic field gradient perpendicular to the current sheet represents only a lower limit of the actual current flowing in this chromospheric current sheet. The width of the valley in the magnetic field strength corresponds to the spatial resolution of 1 × 10^6 m, limited by turbulence in the Earth's atmosphere, so that the horizontal gradient of the magnetic field is underestimated.

sheet. The maximum value of 90 mA m^{-2} is a lower limit, because we do not resolve the current sheet.

This is, to our knowledge, the first direct evidence of an electric current sheet in the upper solar atmosphere, whose presence has long been predicted. Currents are usually deduced from photospheric vector magnetograms[14]. Outside sunspots the interpretation of the photospheric currents is not straightforward, because there the field is highly filamented and unresolved. In the upper chromosphere it has expanded to fill all of space, so that an interpretation in terms of a current sheet is reasonable. Current sheets are thought to be formed spontaneously when the footprints of the Sun's magnetic field are shuffled around[3,4,15] or when new magnetic flux emerges into the solar atmosphere. Our observations demonstrate that vector spectropolarimetry of the He I 1083.0 nm line allows such current sheets to be detected, thus providing the possibility of observationally testing their importance for the triggering of flares or for coronal heating[16]. The presence of such a clear signature in the very first magnetic vector map made with the He I line provides strong support for coronal heating theories based on magnetic energy dissipation at current sheets. □

Received 21 March; accepted 2 September 2003; doi:10.1038/nature02035.

1. Yokoyama, T. & Shibata, K. Magnetic reconnection as the origin of X-ray jets and H-alpha surges in the Sun. *Nature* **375,** 42–44 (1995).
2. Lites, B. W., Skumaniah, A. & Martínez Pillet, V. Vector magnetic fields of emerging solar flux. I. Properties at the site of emergence. *Astron. Astrophys.* **333,** 1053–1068 (1998).
3. Parker, E. N. Magnetic neutral sheets in evolving fields—Part One—General theory. *Astrophys. J.* **264,** 635–641 (1983).
4. Parker, E. N. Magnetic neural sheets in evolving fields—Part Two—Formation of the solar corona. *Astrophys. J.* **264,** 642–647 (1983).
5. Parker, E. N. Nanoflares and the solar X-ray corona. *Astrophys. J.* **330,** 474–479 (1988).
6. Ulmschneider, P., Priest, E. R. & Rosner, R. (eds) *Mechanism of Chromospheric and Coronal Heating* Ch. 4 (Springer, Berlin/Heidelberg/New York, 1991).
7. Mártinez Pillet, V. *et al.* in *ASP Conf. Ser. 183. High Resolution Solar Physics: Theory, Observation, and Techniques* 264 (Astronomical Society of the Pacific, San Francisco, California, 1999).
8. Harvey, J. & Hall, D. in *IAU Symp. 43. Solar Magnetic Fields* (ed. Howard, R.) 279–288 (Dordrecht, Reidel, 1971).
9. Penn, M. J. & Kuhn, J. R. Imaging spectropolarimetry of the He I 1083 nanometer line in a flaring solar active region. *Astrophys. J.* **441,** L51–L54 (1995).
10. Rüedi, I., Solanki, S. K. & Livingston, W. C. Infrared lines as probes of solar magnetic features. X. He I 10830A as a diagnostic of chromospheric magnetic fields. *Astron. Astrophys.* **293,** 252–262 (1995).
11. Rüedi, I., Keller, C. U. & Solanki, S. K. Measurements of the full Stokes vector of He I 10830 A. *Sol. Phys.* **164,** 265–275 (1996).
12. Handy, B. N. *et al.* The transition region and coronal explorer. *Sol. Phys.* **187,** 229–260 (1999).
13. Schmidt, W., Muglach, K. & Knölker, M. Free-fall downflow observed in He I 1083.0 nanometers and Hβ. *Astrophys. J.* **544,** 567–571 (2000).
14. Zirin, H. & Wang, H. Narrow lanes of transverse magnetic field in sunspots. *Nature* **363,** 426–428 (1993).
15. Galsgaard, K. & Longbottom, A. W. Formation of solar prominences by flux convergence. *Astrophys. J.* **510,** 444–459 (1999).
16. Gudiksen, B. V. & Nordlund, Å. Bulk heating and slender magnetic loops in the solar corona. *Astrophys. J.* **572,** L113–L116 (2002).
17. Ruiz Cobo, B. & del Toro Iniesta, J. C. Inversion of Stokes profiles. *Astrophys. J.* **398,** 375–385 (1992).
18. Frutiger, C., Solanki, S. K., Fligge, M. & Bruls, J. H. M. J. Properties of the solar granulation obtained from the inversion of low spatial resolution spectra. *Astron. Astrophys.* **358,** 1109–1121 (2000).
19. Kurucz, R. L. 'Finding' the 'Missing' solar ultraviolet opacity. *Rev. Mexicana Astron. Astrofis.* **23,** 181–186 (1992).
20. Avrett, E. H., Fontenla, J. M. & Loeser, R. in *IAU Symp. 154. Infrared Solar Physics* (ed. Rabin, D. M.) 35–47 (Kluwer Academic, Dordrecht, 1994).
21. Giovanelli, R. G. & Hall, D. The helium 10830 A line in the undisturbed chromosphere. *Sol. Phys.* **52,** 211–228 (1977).
22. Rachkowsky, D. N. The reduction for anomalous dispersion in the theory of the absorption line formation in a magnetic field [in Russian]. *Izv. Krym. Astrofiz. Obs.* **37,** 56–61 (1967).
23. Trujillo Bueno, J., Landi Degl'Innocenti, E., Collados, M., Merenda, L. & Manso Sainz, R. Selective absorption processes as the origin of puzzling spectral line polarization from the Sun. *Nature* **415,** 403–406 (2002).
24. Lagg, A., Woch, J., Krupp, N. & Solanki, S. K. Retrieval of the full magnetic vector with the He I multiplet at 1083 nm. *Astron. Astrophys.* (submitted).

Acknowledgements M.C. acknowledges support from the Spanish Ministerio de Ciencia y Tecnologia. We thank the Kiepenheuer Institut in Freiburg, Germany, for observing support.

Competing interests statement The authors declare that they have no competing financial interests.

Correspondence and requests for materials should be addressed to S.K.S. (solanki@linmpi.mpg.de).

The speed of information in a 'fast-light' optical medium

Michael D. Stenner[1], Daniel J. Gauthier[1] & Mark A. Neifeld[2]

[1]*Duke University, Department of Physics, and The Fitzpatrick Center for Photonics and Communication Systems, Durham, North Carolina 27708, USA*
[2]*Department of Electrical and Computer Engineering, The Optical Sciences Center, University of Arizona, Tucson, Arizona 85721, USA*

One consequence of the special theory of relativity is that no signal can cause an effect outside the source light cone, the space-time surface on which light rays emanate from the source[1]. Violation of this principle of relativistic causality leads to paradoxes, such as that of an effect preceding its cause[2]. Recent experiments on optical pulse propagation in so-called 'fast-light' media—which are characterized by a wave group velocity v_g exceeding the vacuum speed of light c or taking on negative values[3]—have led to renewed debate about the definition of the information velocity v_i. One view is that $v_i = v_g$ (ref. 4), which would violate causality, while another is that $v_i = c$ in all situations[5], which would preserve causality. Here we find that the time to detect information propagating through a fast-light medium is slightly longer than the time required to detect the same information travelling through a vacuum, even though v_g in the medium vastly exceeds c. Our observations are therefore consistent with relativistic causality and help to resolve the controversies surrounding superluminal pulse propagation.

The speed of a light pulse travelling through an optical material is not precisely defined, because any pulse comprises a collection of elementary sinusoidal waveforms, each with a distinct frequency ω. Each constituent sinusoid travels at a well-defined velocity known as the phase velocity $v_p = c/n(\omega)$, where $n(\omega)$ is the refractive index of the optical material. Approximate theories of optical pulse propagation predict that the peak travels at the group velocity $v_g = c/(n + \omega\, dn/d\omega|_{\omega=\omega o}) = c/n_g$, where n_g is the group index and ω_o is the central frequency of the wavepacket[6].

We refer to the quantity $dn/d\omega$ as the dispersion of an optical material. For typical optical materials, there exist narrow spectral regions where $n(\omega)$ is a decreasing function of frequency (that is, $dn/d\omega < 0$), resulting in a condition known as anomalous dispersion[7]. When ω_o is within such a region, n_g can be less than one and can even become negative when the anomalous dispersion is large. This results in 'fast light', for which it is possible that the peak of a light pulse may exit the optical material before it passes through the entrance face[8]. The amount of fast-light pulse advancement is largest when v_g is negative and near zero (n_g large and negative).

The possibility of superluminal group velocities ($v_g > c$ or $v_g < 0$) was such a concern to researchers around 1910 that several conference sessions were devoted to the topic[9]. Based on these discussions, Sommerfeld demonstrated theoretically that the velocity of the front of a square-shaped pulse propagating through any medium is identically equal to c and hence relativistic causality is preserved[10]. In a follow-up study, Brillouin suggested that the group velocity is not physically meaningful when the dispersion is anomalous because the pulse becomes severely distorted[11]. More recent research investigating the propagation of smooth-shaped pulses has shown that this conclusion is not justified, leading to renewed controversy[8,12–20].

Another outcome of the discussions in the early 1900s, as recounted in the preface and first chapter of the book by Brillouin[9], was a reformulation of the fundamental postulate of the special theory of relativity. This reformulation states that, rather than limiting the speed of an 'object', it is the information velocity v_i that is limited by c. Unfortunately, there is no agreed-upon definition of the information velocity[2].